VEGA/CHARA interferometric observations of Cepheids

I. A resolved structure around the prototype classical Cepheid δ Cep in the visible spectral range[*]

N. Nardetto[1], A. Mérand[2], D. Mourard[1], J. Storm[3], W. Gieren[4,5], P. Fouqué[6], A. Gallenne[2,4],
D. Graczyk[4,5,7], P. Kervella[8,9], H. Neilson[10], G. Pietrzynski[7], B. Pilecki[7], J. Breitfelder[8], P. Berio[1],
M. Challouf[1,11], J.-M. Clausse[1], R. Ligi[1], P. Mathias[12,13], A. Meilland[1], K. Perraut[14,15], E. Poretti[16],
M. Rainer[16], A. Spang[1], P. Stee[1], I. Tallon-Bosc[17], and T. ten Brummelaar[18,19]

(Affiliations can be found after the references)

ABSTRACT

Context. The B-W method is used to determine the distance of Cepheids and consists in combining the angular size variations of the star, as derived from infrared surface-brightness relations or interferometry, with its linear size variation, as deduced from visible spectroscopy using the projection factor. The underlying assumption is that the photospheres probed in the infrared and in the visible are located at the same layer in the star whatever the pulsation phase. While many Cepheids have been intensively observed by infrared beam combiners, only a few have been observed in the visible.

Aims. This paper is part of a project to observe Cepheids in the visible with interferometry as a counterpart to infrared observations already in hand.

Methods. Observations of δ Cep itself were secured with the VEGA/CHARA instrument over the full pulsation cycle of the star.

Results. These visible interferometric data are consistent in first approximation with a quasi-hydrostatic model of pulsation surrounded by a static circumstellar environment (CSE) with a size of $\theta_{CSE} = 8.9 \pm 3.0$ mas and a relative flux contribution of $f_{CSE} = 0.07 \pm 0.01$. A model of visible nebula (a background source filling the field of view of the interferometer) with the same relative flux contribution is also consistent with our data at small spatial frequencies. However, in both cases, we find discrepancies in the squared visibilities at high spatial frequencies (maximum 2σ) with two different regimes over the pulsation cycle of the star, $\phi = 0.0-0.8$ and $\phi = 0.8-1.0$. We provide several hypotheses to explain these discrepancies, but more observations and theoretical investigations are necessary before a firm conclusion can be drawn.

Conclusions. For the first time we have been able to detect in the visible domain a resolved structure around δ Cep. We have also shown that a simple model cannot explain the observations, and more work will be necessary in the future, both on observations and modelling.

Key words. techniques: interferometric – circumstellar matter – stars: oscillations

1. Introduction

The Baade-Wesselink (BW) method for the distance determination of Cepheids is, in its first version, purely spectro-photometric (Lindemann 1918; Baade 1926; Wesselink 1946). Results by Fouqué et al. (2007) and Storm et al. (2011a,b) illustrate the central and current role of this method in the distance scale calibration, even if recent calibrations of the Hubble constant rely exclusively on the trigonometric parallaxes of a few Galactic Cepheids (Riess et al. 2011; Benedict et al. 2007). The first interferometric version of the BW method was attempted in the visible by Mourard et al. (1997), and soon afterward in the infrared by Kervella et al. (1999, 2001) and Lane et al. (2000). Since then, the infrared interferometric BW method has been applied to a significant number of Cepheids, twelve in total (see Table 1), while among these stars only four have been observed by visible interferometers, and the pulsation could actually be resolved for only one of them, ℓ Car (Davis et al. 2009).

The principle of the interferometric version of the BW method is simple. Interferometric measurements lead to angular diameter estimations over the whole pulsation period, while the stellar radius variations can be deduced from the integration of the pulsation velocity. The latter is linked to the observational velocity deduced from spectral line profiles by the projection factor p (Nardetto et al. 2004; Mérand et al. 2005; Nardetto et al. 2007, 2009).

There are several underlying assumptions to the BW method. First, the limb-darkening of the star is assumed to be constant during the pulsation cycle. This has no impact on the interferometric analysis, at least in the infrared (Kervella et al. 2004), while in the visible Davis et al. (2009) reported the need to take into account a limb-darkening variation from Sydney University Stellar Interferometer (SUSI) observations. On the theoretical side, Nardetto et al. (2006a) found via hydrodynamical simulation that considering a constant limb darkening in the visible leads to a systematic shift of about 0.02 in phase on the angular diameter curve, which basically means that there is no impact on the derived distance (because the amplitude of the angular diameter curve is unchanged). Second, the projection-factor, mostly dominated by the limb-darkening calculated in the visible

---

Table 1. Cepheids for which an interferometric BW method has been applied.

Cepheids	Reference
visible	
δ Cep*	Mourard et al. (1997)
α UMi*, ζ Gem*, δ Cep*, η Aql*	Nordgren et al. (2000)
δ Cep*, η Aql*	Armstrong et al. (2001)
ℓ Car	Davis et al. (2009)
H band	
ζ Gem	Lane et al. (2000)
ζ Gem, η Aql	Lane et al. (2002)
κ Pav	Breitfelder et al. (2015)
ℓ Car	Anderson et al. (2016)
X Sgr, W Sgr, ζ Gem, β Dor, ℓ Car	Breitfelder et al. (2016)
K band	
ζ Gem*	Kervella et al. (2001)
X Sgr*, η Aql, W Sgr, ζ Gem*, β Dor, Y Oph*, ℓ Car	Kervella et al. (2004)
δ Cep	Mérand et al. (2005)
Y Oph	Mérand et al. (2007)
FF Aql, T Vul	Gallenne et al. (2012)
δ Cep, η Aql	Merand et al. (2015a)

Notes. For some studies corresponding to the first attempts (indicated by asterisks) the pulsation could not be clearly resolved angularly leading to a mean value of the angular diameter of the Cepheid. In the visible domain, the BW method was applied successfully to only one Cepheid, ℓ Car, while in the infrared, among the eleven Cepheids the pulsation could be resolved for all stars, even X Sgr, which is known to be atypical likely owing to shockwaves travelling within the atmosphere (Mathias et al. 2006).

domain, is also assumed to be constant, which seems reasonable, at least in theory (Nardetto et al. 2004). Third, when applying the BW method, visible spectroscopy (e.g. Nardetto et al. 2006b) is often combined with infrared interferometric data, or even – in the recent photometric version of the BW method – with various photometric bands (Breitfelder et al. 2015). In the distance determination, we implicitly assume that the angular and linear diameters correspond to the same physical layer in the star. In this context, testing these hypotheses using visible interferometric observations seems to be of prime importance. This can be done first by simply verifying the internal consistency of the BW distances derived from visible and infrared interferometry, and then comparing them with available precise parallaxes (Benedict et al. 2007; Majaess et al. 2012).

This paper is the first in a series which investigates Cepheids with the Visible spEctroGraph and polArimeter (VEGA) beam combiner (Mourard et al. 2009) operating at the focus of the Center for High Angular Resolution Astronomy (CHARA) array (ten Brummelaar et al. 2005) located at the Mount Wilson Observatory (California, USA). The study focuses on the prototype δ Cep star. The VEGA data are first reduced (Sect. 2) and then analysed in terms of uniform disk angular diameters (Sect. 3). In Sect. 4, we show that δ Cep is clearly surrounded by a resolved structure, while some evidence in our interferometric data point toward an additional physical effect. We explore two hypotheses: a circumstellar reverberation and a strong limb-darkening variation. We draw our conclusions in Sect. 5.

2. VEGA/CHARA observations of δ Cep

The CHARA array consists of six telescopes of 1 m in diameter, spread in a Y-shaped configuration, which offers 15 different baselines from 34 m to 331 m. These baselines can achieve a spatial resolution up to 0.3 mas in the visible. The interferometric observations were secured with the VEGA/CHARA instrument.

The journal of observations is presented in Tables A.1 to A.2. Given the large angular size of δ Cep, we used only two short baselines, i.e. S1S2 and E1E2, with projected baselines ranging from about 27 to 31 m for S1S2 and from 52 to 66 m for E1E2. The data were processed using the standard VEGA pipeline (Mourard et al. 2009, 2011; Ligi et al. 2013) considering different spectral bands from 3 nm (in high spectral resolution mode) to 20 nm (in medium spectral resolution mode), and with reference wavelengths ranging from 500 nm to 745 nm (the minimum and maximum wavelengths of these bands are given in Tables A.1 to A.2).

In order to calibrate the squared visibilities, we considered the references stars HD 214734 (C1) and HD 213558 (C2). The first was used to calibrate the data of β Cep presented in Nardetto et al. (2011). Several nights of VEGA observations in 2008 and 2009 were also devoted to controlling the quality of these calibrators by comparing their transfer functions (defined as the ratio of the actual to expected squared visibility) with those of six other calibrators listed in Table 2 (hereafter C3 to C8). The consistency among the eight calibrators is shown in Fig. A.1, while the general quality of VEGA/CHARA data is illustrated in Fig. A.2.

Cycle-to-cycle variations have never been detected for δ Cep, although they have been for a few other Cepheids (Anderson 2014; Anderson et al. 2016). The data are thus recomposed into a unique cycle and the data corresponding to nights that are close in pulsation phase are merged (see phases 0.180, 0.526, 0.627 in Tables A.1 to A.2). Delta Cephei was finally observed on 20 separate nights corresponding to 17 different pulsation phases. As the observations over a given night can be spread over several hours, we first derive the phase for each observation during the night and then calculate the average and the corresponding standard deviation. The standard deviations of the pulsation phases are rather low and range from 0.001 to 0.017, except for $\phi = 0.999$ where we get an error of 0.025 because the

Table 2. List and properties of calibration stars selected with the *SearchCal* software provided by the Jean-Marie Mariotti Center (JMMC) (Bonneau et al. 2006, 2011).

Calibrator HD	Number	Spectral type	T_{eff} K	$\log g$ [cgs]	R	θ_{UD} (R band) [mas]
HD 214734	C1	A3IV	8600	4.2	5.073	0.327 ± 0.023
HD 213558	C2	A1V	9500	4.1	3.770	0.458 ± 0.033
HD 195725	C3	A7III	8000	3.3	4.050	0.617 ± 0.044
HD 182564	C4	A2IIIs	9380	3.4	4.550	0.377 ± 0.027
HD 211336	C5	F0IV	7300	4.3	3.920	0.714 ± 0.051
HD 214454	C6	A8IV	7500	4.3	4.410	0.581 ± 0.042
HD 3360	C7	B2IV	20 900	3.9	3.740	0.284 ± 0.020
HD 192907	C8	B9III	10 500	3.4	4.410	0.346 ± 0.025

Notes. T_{eff} is the effective temperature, g the gravitation acceleration, R the magnitude of the calibrator in the Johnson R filter, θ_{UD} the uniform disk angular diameter for the R filter of the Johnson photometric system. These parameters were adopted from Lafrasse et al. (2010) for all calibrators, except HD 195725 (C3) for which we used the *SearchCal* tool itself. C1 and C2 were used in this study to calibrate the δ Cep VEGA/CHARA data (see Fig. A.2), while C3 to C8 were used to test the robustness of the C1 and C2 calibrators (see Fig. A.1).

star was observed at the very beginning and at the very end of the night. The pulsation phases can be found in Table 3 together with their respective errors, the number of visibility measurements (N), and the baseline used. For each calibrated visibility, the statistical and systematic calibration errors are given separately. The systematic calibration errors, owing to the uncertainty on the estimation of the diameter of the reference star, were found to be negligible compared to the statistical values. Therefore, we only considered the statistical uncertainties in the model fitting. In a few cases, the statistical uncertainty was clearly underestimated. Thus, we fixed the uncertainty on the calibrated squared visibility to 0.05 (Mourard et al. 2012) for the following nights: 2012 September 23, 2013 October 26, 2013 November 26, 2014 July 02, 2014 July 05, and 2014 July 09.

3. Uniform disk (UD) angular diameters

In Figs. A.3, the calibrated visibilities corresponding to E1E2 measurements are plotted as a function of the spatial frequency together with the corresponding (u,v) coverage and for each pulsation phase. We fit these calibrated visibilities by a uniform disk using a JMMC[1] tool, *LITpro* (Tallon-Bosc et al. 2008). The results are given in Table 3 and plotted in Fig. 1 with blue crosses. The data corresponding to S1S2 measurements are shown in Fig. 2a. Owing to their low spatial frequencies, these S1S2 measurements are almost not sensitive to the pulsation of the star. This can be seen in Fig. 2b. Moreover, we have only a few S1S2 measurements per pulsation phase (four at most). Consequently, as a point of comparison with the E1E2 data, we merge the S1S2 data and fit them with a uniform disk angular diameter. The result is given in Table 3 and plotted in Fig. 1 by a horizontal dashed zone. For the data of 2014 October 24, which include both E1E2 and S1S2 baselines, we made two fits, one including all the S1S2 data and another with the E1E2 data. We overplot the very precise K-band uniform disk angular diameter curve obtained by Mérand et al. (2005) (magenta dots). To analyse our VEGA/CHARA angular diameter measurements, we consider the Spectroscopy-Photometry-Interferometry for Pulsating Stars algorithm (SPIPS; Merand et al. 2015a). The SPIPS code combines all the available observables of δ Cep: radial velocimetry (Bersier et al. 1994; Storm et al. 2004), interferometry (FLUOR/CHARA data), and photometry in

Table 3. Pulsation phases, number of visibility measurements (N), resulting uniform disk angular diameters, and reduced χ^2.

ϕ	N	θ_{UD} [mas]	χ^2_{red}	Baseline
0.300	2			S1S2
0.543$_{\pm0.009}$	4	1.705$_{\pm0.035}$	0.9	S1S2
0.666$_{\pm0.006}$	3			S1S2
0.821$_{\pm0.012}$	3			S1S2
0.180$_{\pm0.006}$	15	1.418$_{\pm0.027}$	1.2	E1E2
0.192$_{\pm0.015}$	7	1.400$_{\pm0.010}$	0.1	E1E2
0.292$_{\pm0.009}$	9	1.454$_{\pm0.022}$	1.6	E1E2
0.401$_{\pm0.003}$	4	1.439$_{\pm0.026}$	4.4	E1E2
0.526$_{\pm0.001}$	12	1.425$_{\pm0.012}$	0.6	E1E2
0.627$_{\pm0.017}$	7	1.436$_{\pm0.019}$	0.6	E1E2
0.741$_{\pm0.003}$	8	1.318$_{\pm0.017}$	2.4	E1E2
0.783$_{\pm0.002}$	15	1.316$_{\pm0.010}$	0.9	E1E2
0.821$_{\pm0.012}$	6	1.393$_{\pm0.025}$	2.2	E1E2
0.848$_{\pm0.007}$	24	1.360$_{\pm0.020}$	3.3	E1E2
0.893$_{\pm0.005}$	30	1.405$_{\pm0.019}$	8.1	E1E2
0.927$_{\pm0.003}$	8	1.353$_{\pm0.029}$	0.9	E1E2
0.942$_{\pm0.007}$	13	1.408$_{\pm0.026}$	1.1	E1E2
0.999$_{\pm0.025}$	8	1.337$_{\pm0.016}$	1.4	E1E2

Notes. The baseline used is also indicated. The pulsation phases are calculated using the ephemeris from Kukarkin et al. (1971): $T_0 = 2\,427\,628.86$ days and $P = 5.3663$ days. There is no error on the phase at 0.300 since the two measurements are from the same date but at different reference wavelengths. The S1S2 data were merged in order to derive a mean uniform disk angular diameter.

the V (Berdnikov & Turner 2002; Engle et al. 2014; Kiss 1998; Moffett & Barnes 1984), J, H, and K bands (Barnes et al. 1997) in order to estimate the projection factor, the variation of the effective temperature, and the H and K band excesses. The data used for the fit for δ Cep have been published in digital form (Merand et al. 2015b). In the list of these outputs, we are particularly interested in the uniform disk angular diameter curves, calculated at 2200 nm and 800 nm, and derived directly from the framework of Merand et al. (2015a). The data are given in Table 4 and are shown in Fig. 1 by red crosses and light blue squares, respectively. In the infrared, the K-band UD angular diameter curve of SPIPS is consistent with the FLUOR/CHARA
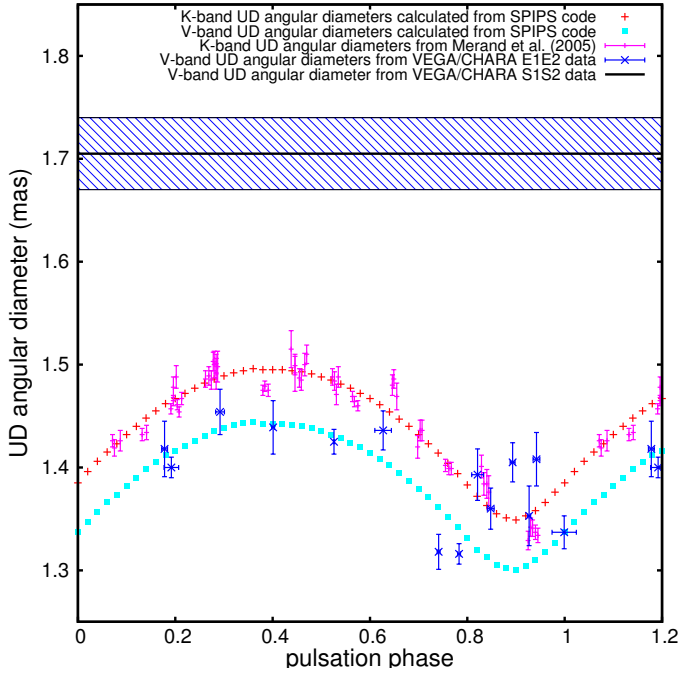
---

[1] http://www.jmmc.fr/litpro

Fig. 1. Uniform disk diameters θ_{UD} derived from the VEGA/CHARA E1E2 data plotted as a function of the pulsation phase (blue crosses). The S1S2 data (corresponding to four different pulsation phases, see Table 3) were merged and the corresponding mean θ_{UD} is represented by a black horizontal line together with the 1σ uncertainty (blue dashed zone). The uniform disk angular diameter curve from FLUOR/CHARA in the K band (Mérand et al. 2005) is also shown for comparison. The red crosses and the light blue squares show the K band and R band UD angular diameter curves, respectively, as predicted from the SPIPS code (Merand et al. 2015a).

measurements. In the visible domain, the reduced χ^2 between the VEGA (E1E2) and SPIPS UD angular diameters is 9, while it increases slightly to 11 when we replace the SPIPS angular diameter variation by a constant corresponding to the average of the VEGA UD angular diameters, i.e. 1.376±0.030 mas. We thus detect a pulsation in the visible band, but make three remarks:

1. The VEGA S1S2 measurements provide a mean θ_{UD} (with a reduced χ^2 of 0.9), which is significantly larger than the E1E2 angular diameter curve by about 10σ. This suggests the presence of a large angular structure around the pulsating Cepheid.
2. The SPIPS predictions are consistent with the VEGA θ_{UD} angular diameters from 0.0 to 0.8 in phase (with a reduced χ^2 of 4). This basically means that δ Cep is pulsating in a quasi-hydrostatic way over this range of pulsation phase, even if the two measurements (at $\phi = 0.741$ and $\phi = 0.783$) are slightly below the SPIPS curve (around 2σ).
3. Five measurements between 0.8 and 1.0 are clearly from 2 to 6σ above the SPIPS curve (with a reduced χ^2 of 8).

4. Detection of a circumstellar environment or a nebulae in the visible

In Fig. 2b, the S1S2 data are fitted with a model (open symbols) composed of the UD derived from the SPIPS UD angular diameter curve at the corresponding phases of VEGA observations and a second static disk describing the circumstellar environment (CSE). The orientation of the S1S2 measurements in the

Table 4. Angular diameters as derived from the application of the SPIPS algorithm to δ Cep, using photometry, interferometry, and the cross-correlated radial velocity curves as inputs (see Merand et al. 2015a).

Phase	θ_{Ross}	$\theta_{UD}[0.8\ \mu m]$	$\theta_{UD}[2.2\ \mu m]$
0.00	1.399	1.337	1.385
0.02	1.409	1.347	1.396
0.04	1.420	1.357	1.406
0.06	1.430	1.366	1.415
0.08	1.439	1.373	1.423
0.10	1.449	1.382	1.432
0.12	1.457	1.390	1.440
0.14	1.465	1.398	1.448
0.16	1.473	1.405	1.455
0.18	1.480	1.412	1.462
0.20	1.487	1.416	1.467
0.22	1.492	1.421	1.472
0.24	1.498	1.426	1.477
0.26	1.502	1.431	1.482
0.28	1.507	1.435	1.486
0.30	1.510	1.438	1.489
0.32	1.513	1.441	1.492
0.34	1.515	1.443	1.494
0.36	1.517	1.444	1.496
0.38	1.518	1.442	1.495
0.40	1.518	1.442	1.495
0.42	1.518	1.442	1.495
0.44	1.517	1.441	1.494
0.46	1.515	1.440	1.493
0.48	1.513	1.438	1.491
0.50	1.511	1.435	1.488
0.52	1.508	1.432	1.485
0.54	1.504	1.429	1.481
0.56	1.499	1.424	1.477
0.58	1.494	1.420	1.472
0.60	1.489	1.414	1.467
0.62	1.482	1.408	1.461
0.64	1.476	1.402	1.454
0.66	1.468	1.395	1.447
0.68	1.460	1.387	1.440
0.70	1.452	1.379	1.432
0.72	1.443	1.371	1.423
0.74	1.433	1.362	1.414
0.76	1.423	1.352	1.404
0.78	1.412	1.342	1.394
0.80	1.401	1.331	1.383
0.82	1.390	1.320	1.372
0.84	1.379	1.313	1.363
0.86	1.370	1.305	1.355
0.88	1.364	1.302	1.351
0.90	1.362	1.300	1.349
0.92	1.365	1.304	1.353
0.94	1.371	1.310	1.358
0.96	1.379	1.318	1.366
0.98	1.389	1.327	1.376
	mas	mas	mas

Notes. θ_{Ross} is the Rosseland angular diameter (provided as an indication, but not used in this paper); $\theta_{UD}[0.8\ \mu m]$ and $\theta_{UD}[2.2\ \mu m]$ are the UD angular diameters calculated at 0.8 and 2.2 μm, respectively. We used a distance d of 274 ± 11 pc (Benedict et al. 2002).
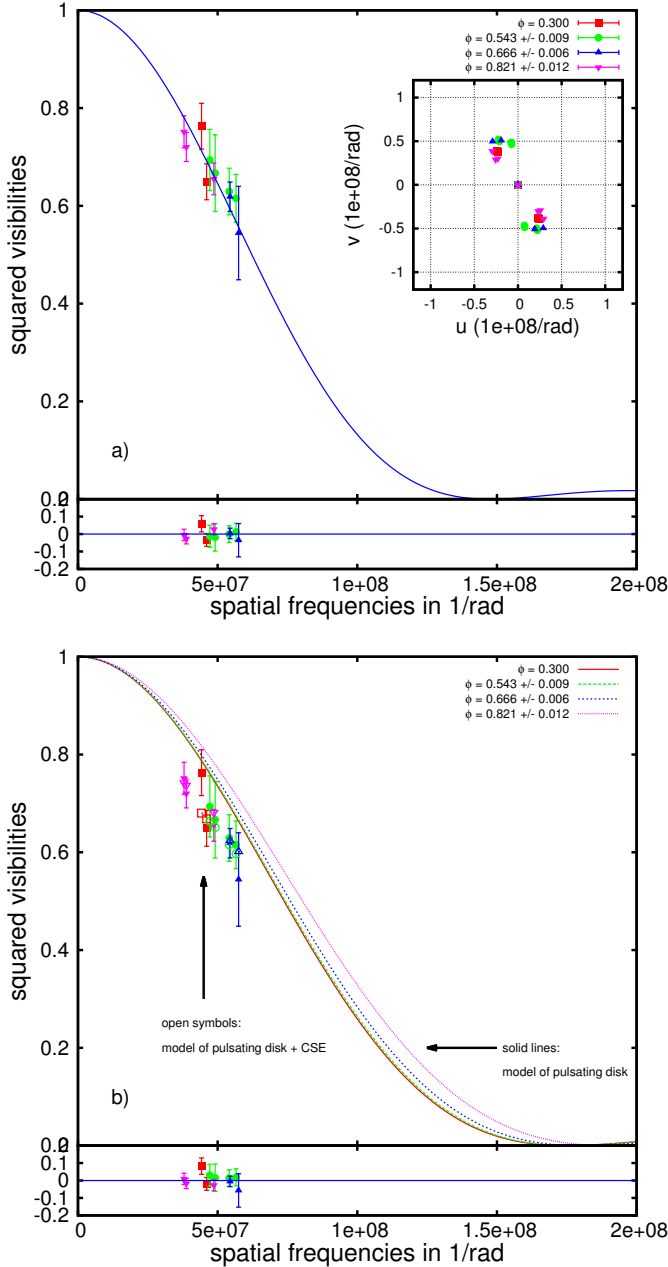
Fig. 2. a) S1S2 observed calibrated squared visibilities secured at four different pulsation phases plotted as a function of the spatial frequency together with the best fit of uniform disk model (solid blue line). In the upper right corner we show the corresponding (u, v) coverage. **b)** Same data fitted with a two-component model (open symbols) including a uniform pulsating disk and a CSE (see text). As a comparison, the solid lines are the corresponding one-component models, i.e. a uniform pulsating disk (in the R band) without the CSE.

(u, v) coverage are between 148 and 171 degrees, preventing us from investigating a non-centrosymmetric CSE. The best-fit parameters are $\theta_{CSE} = 8.9 \pm 3.0$ mas (the size of the CSE) and $\frac{f_{cse}}{f_\star} = 0.07 \pm 0.01$ (the relative flux contribution of the CSE, where f_{cse} and $f_\star$ are the fluxes of the CSE and the star in the R band, respectively) with a reduced χ^2 of 0.6. The two parameters, however, are significantly correlated (0.8) owing to the low number of S1S2 observations. Interestingly, we can also fit the S1S2 data (with the same reduced χ^2 of 0.6) using a model composed of a pulsating disk, as in the previous case, together with a background contribution of 0.07 ± 0.01 in flux filling

the field of view of the interferometer. This model physically corresponds to the visible counterpart of the infrared nebulae discovered by Marengo et al. (2010) and the HI nebula found with the Very Large Array (VLA) (Matthews et al. 2012). Unfortunately, our S1S2 data are too scarce to distinguish between these two hypotheses.

We have fitted the S1S2 data with a two-component model without considering the E1E2 data. Hence, we now have to verify whether this two-component model is consistent with our E1E2 data, in particular at minimum radius. In Sect. 3, we find that the E1E2 measurements are not consistent with a quasi-hydrostatic pulsating disk at the minimum radius of the star (between phase 0.8 and 1.0).

In order to address this issue, we plot in panel a) of Fig. 3 all the VEGA visibilities measured as a function of $x = \frac{\pi B_{\rm p}[{\rm m}]\theta_{\rm UD}[{\rm mas}]}{\lambda[{\rm nm}]}$, where $\theta_{\rm UD}$ is fixed and interpolated from the SPIPS UD angular diameter curve at the corresponding pulsation phase of VEGA observations. The data are rescaled in such a way that they can be compared, despite different $\theta_{\rm UD}$ (or pulsation phases) and different wavelengths of observation. This is possible since the reference is the SPIPS $\theta_{\rm UD}$ semi-theoretical curve represented by the solid blue line expressed by $V^2(x) = |\frac{2J_1(x)}{x}|$, where J_1 is the Bessel function of the first order. This concept of pseudo-baseline was first introduced by Mérand et al. (2006). Using this approach, we confirm the three statements found in Sect. 3:

1. The S1S2 measurements, whatever the pulsation phase, are significantly lower than in the rescaled uniform disk model (see the S1S2 measurements, i.e. data with x from approximately 0.5 to 1.4, Fig. 3b). This deviation is removed as soon as we consider a resolved structure around δ Cep (see below).
2. The data with a pulsating phase from $\phi = 0.0$ to $\phi = 0.8$ are consistent with the uniform disk model for E1E2 measurements (blue crosses with x from 1.5 to 2.8 in Fig. 3b).
3. The data with a pulsating phase from $\phi = 0.8$ to $\phi = 1.0$ are not consistent with the uniform disk model for E1E2 measurements (green circles around $x = 1.7$ in Fig. 3b).

In Fig. 3a, we overplot a red dotted line to the squared visibility curve corresponding to a uniform disk surrounded by the CSE using the formula

$$V^2(x) = \left(f_\star \left| \frac{2J_1(x)}{x} \right| + f_{cse} \left| \frac{2J_1(s_{\rm r}x)}{s_{\rm r}x} \right| \right)^2, \qquad (1)$$

where $f_{cse} = 0.065$ and $f_\star = 0.935$ (corresponding to $\frac{f_{cse}}{f_\star} = 0.07 \pm 0.01$ and $f_{cse} + f_\star = 1$), $s_{\rm r}$ is the mean size ratio between the CSE and the pulsating disk. Considering the mean UD angular diameter of the SPIPS curve ($\theta_{mean} = 1.39$ mas), we find $s_{\rm r} = 6.32$. The result is unchanged (i.e. within the width of the line) if we use the 6.75 and 6.07 values corresponding to the minimum and maximum UD angular diameters.

We find that the S1S2 measurements are properly fitted by this two-component model, as expected (Fig. 3c). However, around $x = 1.7$ the E1E2 measurements corresponding to $\phi = 0.0{-}0.8$ and $\phi = 0.8{-}1.0$ are respectively above and below the curve (by about 2σ). All the E1E2 measurements are partly above the curve (about 1σ) at larger frequencies ($x > 2.3$).

If we consider the model composed of a uniform disk surrounded by a background, we obtain

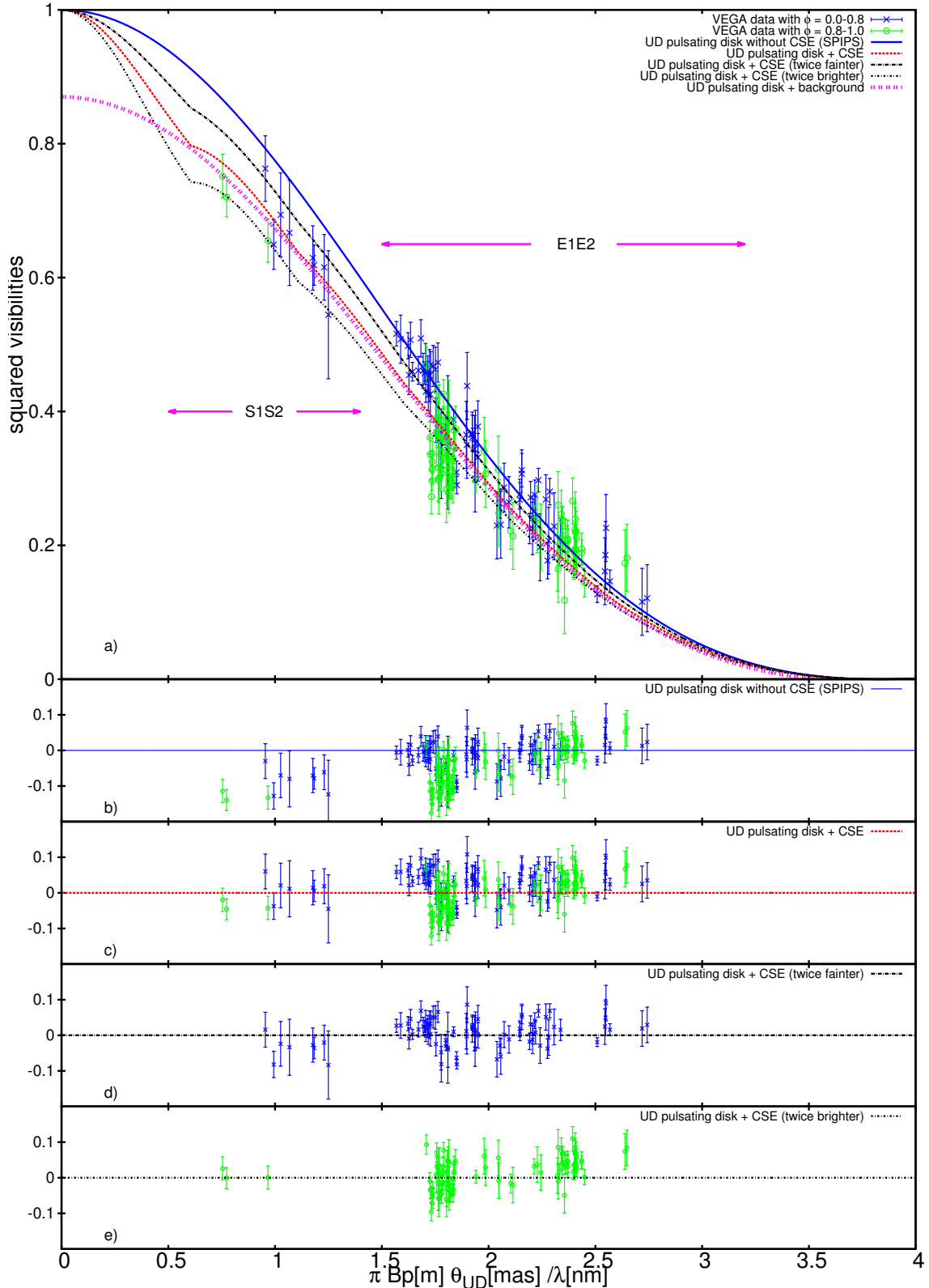$$V^2(x) = \left(f_\star \left| \frac{2J_1(x)}{x} \right| \right)^2 - f_{cse}^2, \qquad (2)$$

Fig. 3. Panel **a)**, the VEGA squared visibilities plotted as a function of $x = \frac{\pi B_p[m]\theta_{UD}[mas]}{\lambda[nm]}$ in order to allow a comparison between data of different phases (i.e. different θ_{UD}) and effective wavelengths. Five models are overplotted: (1) the UD pulsating disk without CSE from the SPIPS algorithm (blue solid line); (2) the SPIPS UD pulsating disk + the CSE from Eq. (1) (red dotted line); (3) the SPIPS UD pulsating disk + the CSE from Eq. (1) but two times brighter (dashed line); (4) the SPIPS UD pulsating disk + the CSE or Eq. (1) but two times fainter (dash-dotted line); (5) the SPIPS UD pulsating disk + a background contribution filling the field of view of the interferometer (magenta dotted line). The residual between the observations and models 1 to 4 are shown in panels **b)**, **c)**, **d)**, and **e)**, respectively. In panels **d)** and **e)** we show only the data corresponding to phases intervals $\phi = 0.0-0.8$ and $\phi = 0.8-1.0$, respectively.

and the corresponding curve is plotted by a magenta dotted line in Fig. 3a. We arrive at the same conclusions as the model of the pulsating uniform disk surrounded by a CSE. In particular, we find the presence of two regimes in phase, even considering a CSE or a background. We explore two hypotheses.

First, we cannot fit all the VEGA measurements at the same time if we consider a CSE two times fainter or brighter (see black dotted and dot-dashed lines in Fig. 3a). Qualitatively, however, it seems that considering a CSE two times fainter between phase 0.0 and 0.8 is a good compromise to fit the S1S2 and E1E2 measurements together, even if not totally satisfactory (see Fig. 3d). To consider a CSE two times brighter between phase 0.8 and 1.0 (when the size of the star is at a minimum, and is hot and bright) helps to fit the data except at large spatial frequencies (see Fig. 3e). If this hypothesis is correct, then the δ Cep would light up its environment (CSE or background) differently at maximum and minimum radius.

The second possibility is to consider that the CSE (or the background) has a constant brightness and that the discrepancy found for E1E2 measurements comes mainly from an additional structure angularly smaller ($\phi = 0.0-0.8$) or larger ($\phi = 0.8-1.0$) in size than the SPIPS θ_{UD} stellar pulsating disk, for instance a strong limb-darkening variation. The limb-darkening coefficient, defined as $k = \frac{\theta_{UD}}{\theta_{LD}}$, is used to convert the θ_{UD} diameters into limb-darkened θ_{LD} angular diameters. The k coefficient variation in the visible band (at 600 nm) and over the cycle of pulsation of the star is found to be from the hydrodynamical model of 0.015 (Nardetto et al. 2006a), which corresponds to about 1%. Similarly, Marengo et al. (2002, 2003) have found a variation for the k-parameter of about 0.01 and 0.02 for ζ Gem and at 570 nm using quasi-hydrostatic and hydrodynamical models, respectively. Also for comparison, Davis et al. (2009) used a phase-dependent k-parameter to analyse their SUSI data of ℓ Car, and found a variation of 0.012. This means typically a 1% difference in θ_{UD}, and thus a 1% difference in x, which corresponds to 0.02 in absolute value around $x = 1.7$ in Fig. 3. Consequently, the limb-darkening variation of δ Cep is one order of magnitude lower than the discrepancies found for the E1E2 measurements. In the case of δ Cep, the theoretical average value of k is of 0.954 (Nardetto et al. 2006a). So far, the only published direct measurement of the limb-darkening coefficient of a Cepheid (in the visible) has been performed by Pilecki et al. (2013) for a Cepheid ($P = 3.80$ d) in an eclipsing binary system in the LMC. They find the limb-darkening effect to be much stronger than expected for a star of that temperature, giving a possible range for k from 0.91 to 0.93, assuming however no temperature dependence. Recently, Gieren et al. (2015) studied another Cepheid in the LMC ($P = 2.99$ d) and found a similar rather strong limb-darkening effect. If we consider the lower k value found by Pilecki et al. (2013), all the E1E2 measurements in Fig. 3 should translate towards lower values of $x - 4\%$ or about 0.06. The measurements in blue crosses in the figure would be better fitted, while green open circles would not (in particular near $x \simeq 1.7$). The limb-darkening effect is probably not the key issue to explain the discrepancy found for the E1E2 measurements.

5. Discussion

We observed δ Cep intensively on twenty nights. The initial purpose of these observations was to apply the BW method, but instead we detected for the very first time a static resolved structure around δ Cep contributing to about 7% of the total flux in the visible. This is not totally surprising as envelopes around

Cepheids have already been discovered by long-baseline interferometry in the K band with VLTI and CHARA (Kervella et al. 2006; Mérand et al. 2006). In addition, four Cepheids have also been observed in the N band with VISIR and MIDI (Kervella et al. 2009; Gallenne et al. 2013) and one with NACO (Gallenne et al. 2011, 2012). Some evidence has also been found using high-resolution spectroscopy (Nardetto et al. 2008). From these observations, the typical size of the envelope of Cepheids seems to be around 3 stellar radii and the flux contribution from 2% to 10% of the continuum in the K band for medium- and long-period Cepheids, respectively, while it is around 10% or more in the N band. However, Mérand et al. (2005) do not mention any contribution from a CSE in the case of δ Cep in their infrared FLUOR data, while Mérand et al. (2006) found an improved agreement with a larger set of data when considering a model with a CSE. They used a ring model 3.54 mas in size, 0.5 mas in width, and with a relative brightness of 1.5%, which is confirmed in Merand et al. (2015a). The processes at work in infrared and in the visible regarding the CSE are different. We expect thermal emission in the infrared and scattering in the visible. It is also worth mentioning that the mid-infrared flux in excess is not necessarily the evidence for mass loss (see e.g. Schmidt 2015) and that the resolved structure we observe around δ Cep, instead of a CSE, could be simply a visible nebulae (also contributing to 7% of the total flux), as reported in the infrared by Marengo et al. (2010) and in the radio domain by Matthews et al. (2012).

Our second result is the presence of an additional second-order discrepancy between the observations and the models (pulsating disk + CSE or pulsating disk + background) at high spatial frequencies, which is not clearly understood. One possibility could be that the star is lighting up its environment differently at minimum ($\phi \simeq 0.8-1.0$) and maximum ($\phi \simeq 0.0-0.8$) radius. This reverberation effect would then be more important in the visible than in the infrared since the contribution in flux of the CSE (or the background) in the visible band is about 7% compared to 1.5% in the infrared. Interestingly, the phase interval from 0.8 to 1.0 is usually disregarded in the infrared surface brightness version of the BW method owing to general poor agreement between spectroscopic and photometric angular diameters (Storm et al. 2011a,b). The other possibility is to consider a *static* environment with a constant brightness in time, but with an additional dynamical effect. However, from the hydrodynamical simulations and observations of Cepheids in eclipsing binary systems, it seems that the limb-darkening effect in the visible band does not vary strongly enough to reproduce the second-order discrepancy found in our interferometric observations. Also possible is a strong compression or shockwave occurring near the photosphere at the minimum radius, which is indeed the layer probed by photometry and interferometry. However, such a shock is not seen in the hydrodynamical code (Nardetto et al. 2004) or in the spectroscopic data, conversely to X Sgr, an atypical Cepheid in which a shockwave has indeed been reported (Mathias et al. 2006). Why this dynamical effect is seen in the visible band and not in the infrared is another pending question in this hypothesis. We also exclude non-radial pulsation, since very accurate space photometry does not support the detection of such modes in Galactic classical Cepheids (e.g. Poretti et al. 2015), and the previous spectroscopic campaigns would have shown up quite easily. Furthermore, Anderson et al. (2015) found the signature of a companion in recent spectroscopic data of δ Cep. The expected flux contribution is supposed to be lower than 1% in the visible, clearly not detectable by VEGA/CHARA. Finally, reverberation seems to be the more

plausible hypothesis. More interferometric data on Cepheids in the visible might shed light on it. In particular, covering the spatial frequencies properly (x from 0.2 to 3) at a unique pulsating phase (maximum and minimum radii) is probably required to go further in the analysis.

References

Anderson, R. I. 2014, A&A, 566, L10
Anderson, R. I., Sahlmann, J., Holl, B., et al. 2015, ApJ, 804, 144
Anderson, R. I., Mérand, A., Kervella, P., et al. 2016, MNRAS, 455, 4231
Armstrong, J. T., Nordgren, T. E., Germain, M. E., et al. 2001, AJ, 121, 476
Baade, W. 1926, Astron. Nachr., 228, 359
Barnes, III, T. G., Fernley, J. A., Frueh, M. L., et al. 1997, PASP, 109, 645
Benedict, G. F., McArthur, B. E., Fredrick, L. W., et al. 2002, AJ, 124, 1695
Benedict, G. F., McArthur, B. E., Feast, M. W., et al. 2007, AJ, 133, 1810
Berdnikov, L. N., & Turner, D. G. 2002, VizieR Online Data Catalog J/ApJS/137/209
Bersier, D., Burki, G., Mayor, M., & Duquennoy, A. 1994, A&AS, 108, 25
Bonneau, D., Clausse, J.-M., Delfosse, X., et al. 2006, A&A, 456, 789
Bonneau, D., Delfosse, X., Mourard, D., et al. 2011, A&A, 535, A53
Breitfelder, J., Kervella, P., Mérand, A., et al. 2015, A&A, 576, A64
Breitfelder, J., Mérand, A., Kervella, P., et al. 2016, A&A, 587, A117
Davis, J., Jacob, A. P., Robertson, J. G., et al. 2009, MNRAS, 394, 1620
Engle, S. G., Guinan, E. F., Harper, G. M., Neilson, H. R., & Remage Evans, N. 2014, ApJ, 794, 80
Fouqué, P., Arriagada, P., Storm, J., et al. 2007, A&A, 476, 73
Gallenne, A., Mérand, A., Kervella, P., & Girard, J. H. V. 2011, A&A, 527, A51
Gallenne, A., Kervella, P., & Mérand, A. 2012, A&A, 538, A24
Gallenne, A., Mérand, A., Kervella, P., et al. 2013, A&A, 558, A140
Gieren, W., Pilecki, B., Pietrzyński, G., et al. 2015, ApJ, 815, 28
Kervella, P., Coudé du Foresto, V., Traub, W. A., & Lacasse, M. G. 1999, in Working on the Fringe: Optical and IR Interferometry from Ground and Space, eds. S. Unwin, & R. Stachnik, ASP Conf. Ser., 194, 22
Kervella, P., Coudé du Foresto, V., Perrin, G., et al. 2001, A&A, 367, 876
Kervella, P., Nardetto, N., Bersier, D., Mourard, D., & Coudé du Foresto, V. 2004, A&A, 416, 941
Kervella, P., Mérand, A., Perrin, G., & Coudé du Foresto, V. 2006, A&A, 448, 623
Kervella, P., Mérand, A., & Gallenne, A. 2009, A&A, 498, 425
Kiss, L. L. 1998, in A Half Century of Stellar Pulsation Interpretation, eds. P. A. Bradley, & J. A. Guzik, ASP Conf. Ser., 135, 173

Kukarkin, B. V., Kholopov, P. N., Pskovsky, Y. P., et al. 1971, in General Catalogue of Variable Stars, 3rd edn.
Lafrasse, S., Mella, G., Bonneau, D., et al. 2010, VizieR Online Data Catalog: II/300
Lane, B. F., Kuchner, M. J., Boden, A. F., Creech-Eakman, M., & Kulkarni, S. R. 2000, Nature, 407, 485
Lane, B. F., Creech-Eakman, M. J., & Nordgren, T. E. 2002, ApJ, 573, 330
Ligi, R., Mourard, D., Nardetto, N., & Clausse, J.-M. 2013, J. Astron. Instrum., 2, 40003
Lindemann, F. A. 1918, MNRAS, 78, 639
Majaess, D., Turner, D., & Gieren, W. 2012, ApJ, 747, 145
Marengo, M., Sasselov, D. D., Karovska, M., Papaliolios, C., & Armstrong, J. T. 2002, ApJ, 567, 1131
Marengo, M., Karovska, M., Sasselov, D. D., et al. 2003, ApJ, 589, 968
Marengo, M., Evans, N. R., Barmby, P., et al. 2010, ApJ, 725, 2392
Mathias, P., Gillet, D., Fokin, A. B., et al. 2006, A&A, 457, 575
Matthews, L. D., Marengo, M., Evans, N. R., & Bono, G. 2012, ApJ, 744, 53
Mérand, A., Kervella, P., Coudé du Foresto, V., et al. 2005, A&A, 438, L9
Mérand, A., Kervella, P., Coudé du Foresto, V., et al. 2006, A&A, 453, 155
Mérand, A., Aufdenberg, J. P., Kervella, P., et al. 2007, ApJ, 664, 1093
Merand, A., Kervella, P., Breitfelder, J., et al. 2015a, A&A, 584, A80
Merand, A., Kervella, P., Breitfelder, J., et al. 2015b, VizieR Online Data Catalog: J/A+A/584/A80
Moffett, T. J., & Barnes, III, T. G. 1984, ApJS, 55, 389
Mourard, D., Bonneau, D., Koechlin, L., et al. 1997, A&A, 317, 789
Mourard, D., Clausse, J. M., Marcotto, A., et al. 2009, A&A, 508, 1073
Mourard, D., Bério, P., Perraut, K., et al. 2011, A&A, 531, A110
Mourard, D., Challouf, M., Ligi, R., et al. 2012, in SPIE Conf. Ser., 8445, 0
Nardetto, N., Fokin, A., Mourard, D., et al. 2004, A&A, 428, 131
Nardetto, N., Fokin, A., Mourard, D., & Mathias, P. 2006a, A&A, 454, 327
Nardetto, N., Mourard, D., Kervella, P., et al. 2006b, A&A, 453, 309
Nardetto, N., Mourard, D., Mathias, P., Fokin, A., & Gillet, D. 2007, A&A, 471, 661
Nardetto, N., Groh, J. H., Kraus, S., Millour, F., & Gillet, D. 2008, A&A, 489, 1263
Nardetto, N., Gieren, W., Kervella, P., et al. 2009, A&A, 502, 951
Nardetto, N., Mourard, D., Tallon-Bosc, I., et al. 2011, A&A, 525, A67
Nordgren, T. E., Armstrong, J. T., Germain, M. E., et al. 2000, ApJ, 543, 972
Pilecki, B., Graczyk, D., Pietrzyński, G., et al. 2013, MNRAS, 436, 953
Poretti, E., Le Borgne, J. F., Rainer, M., et al. 2015, MNRAS, 454, 849
Riess, A. G., Macri, L., Casertano, S., et al. 2011, ApJ, 730, 119
Schmidt, E. G. 2015, ApJ, 813, 29
Storm, J., Carney, B. W., Gieren, W. P., et al. 2004, A&A, 415, 531
Storm, J., Gieren, W., Fouqué, P., et al. 2011a, A&A, 534, A94
Storm, J., Gieren, W., Fouqué, P., et al. 2011b, A&A, 534, A95
Tallon-Bosc, I., Tallon, M., Thiébaut, E., et al. 2008, in SPIE Conf. Ser., 7013
ten Brummelaar, T. A., McAlister, H. A., Ridgway, S. T., et al. 2005, ApJ, 628, 453
Wesselink, A. J. 1946, Bull. Astron. Inst. Netherlands, 10, 91

[1] Université Côte d'Azur, Observatoire de la Côte d'Azur, CNRS, Laboratoire Lagrange, UMR7293, Nice, France
e-mail: Nicolas.Nardetto@oca.eu
[2] European Southern Observatory, Alonso de Córdova 3107, Casilla 19001, Santiago 19, Chile
[3] Leibniz Institute for Astrophysics, An der Sternwarte 16, 14482 Potsdam, Germany
[4] Departamento de Astronomía, Universidad de Concepción, Casilla 160-C, Concepción, Chile
[5] Millenium Institute of Astrophysics, Santiago, Chile
[6] Observatoire Midi-Pyrénées, Laboratoire d'Astrophysique, UMR 5572, Université Paul Sabatier – Toulouse 3, 14 avenue Édouard Belin, 31400 Toulouse, France
[7] Nicolaus Copernicus Astronomical Center, Polish Academy of Sciences, ul. Bartycka 18, 00-716 Warszawa, Poland
[8] LESIA (UMR 8109), Observatoire de Paris, PSL, CNRS, UPMC, Univ. Paris-Diderot, 5 place Jules Janssen, 92195 Meudon, France

[9] Unidad Mixta Internacional Franco-Chilena de Astronomía, CNRS/INSU, France (UMI 3386) and Departamento de Astronomía, Universidad de Chile, Camino El Observatorio 1515, Las Condes, Santiago, Chile

[10] Department of Astronomy & Astrophysics, University of Toronto, 50 St. George Street, Toronto, ON, M5S 3H4 , Canada

[11] Laboratoire Dynamique Moléculaire et Matériaux Photoniques, UR11ES03, Université de Tunis/ESSTT, Tunisie

[12] Université de Toulouse, UPS-OMP, Institut de recherche en Astrophysique et Planétologie, Toulouse, France

[13] CNRS, UMR5277, Institut de recherche en Astrophysique et Planétologie, 14 avenue Édouard Belin, 31400 Toulouse, France

[14] Université Grenoble Alpes, IPAG, 38000 Grenoble, France

[15] CNRS, IPAG, 38000 Grenoble, France

[16] INAF–Osservatorio Astronomico di Brera, via E. Bianchi 46, 23807 Merate (LC), Italy

[17] Université de Lyon, Université Lyon 1, École Normale Supérieure de Lyon, CNRS, Centre de Recherche Astrophysique de Lyon UMR5574, 69230 Saint-Genis-Laval, France

[18] Georgia State University, PO Box 3969, Atlanta GA 30302-3969, USA

[19] CHARA Array, Mount Wilson Observatory, 91023 Mount Wilson CA, USA

Appendix A: VEGA observations: Log, transfer functions, and visibility curves

Table A.1. Observing log with the E1E2 baseline.

	Date [yyyy.mm.dd]	RJD [days]	HA [hour]	λ_{min} [nm]	λ_{max} [nm]	Bp [m]	PA [deg]	S/N	$V^2_{\mathrm{cal}\pm\mathrm{stat}\pm\mathrm{syst}}$
$\phi = 0.180 \pm 0.006$	2013.10.26	56 591.755	2.19	535	555	65.85	−149.17	5	$0.226_{\pm0.050\pm0.003}$
	2013.10.26	56 591.755	2.19	710	730	65.85	−149.16	7	$0.352_{\pm0.050\pm0.003}$
	2013.10.26	56 591.755	2.19	725	745	65.85	−149.16	9	$0.438_{\pm0.050\pm0.003}$
	2013.10.26	56 591.770	2.55	535	555	65.79	−153.92	4	$0.186_{\pm0.050\pm0.003}$
	2013.10.26	56 591.770	2.55	710	730	65.79	−153.91	6	$0.300_{\pm0.050\pm0.002}$
	2013.10.26	56 591.770	2.55	725	745	65.79	−153.91	7	$0.350_{\pm0.050\pm0.003}$
	2013.10.26	56 591.785	2.91	535	555	65.72	−158.70	3	$0.161_{\pm0.050\pm0.002}$
	2013.10.26	56 591.785	2.91	710	730	65.72	−158.70	7	$0.344_{\pm0.050\pm0.003}$
	2013.10.26	56 591.785	2.91	725	745	65.72	−158.70	7	$0.365_{\pm0.050\pm0.003}$
	2014.07.05	56 843.917	−1.27	730	750	62.08	−106.85	6	$0.320_{\pm0.050\pm0.002}$
	2014.07.05	56 843.933	−0.87	730	750	63.14	−111.65	4	$0.354_{\pm0.050\pm0.002}$
	2014.07.05	56 843.958	−0.17	490	510	64.52	−120.01	2	$0.116_{\pm0.050\pm0.002}$
	2014.07.05	56 843.958	−0.16	660	680	64.53	−120.02	5	$0.230_{\pm0.050\pm0.002}$
	2014.07.05	56 843.979	0.26	490	510	65.09	−125.08	2	$0.121_{\pm0.050\pm0.002}$
	2014.07.05	56 843.979	0.26	660	680	65.10	−125.09	5	$0.231_{\pm0.050\pm0.002}$
$\phi = 0.192 \pm 0.015$	2012.09.24	56 194.645	−2.49	547	560	57.61	−91.87	7	$0.241_{\pm0.050\pm0.002}$
	2012.09.24	56 194.645	−2.51	710	730	57.53	−91.65	28	$0.457_{\pm0.050\pm0.002}$
	2012.09.24	56 194.645	−2.51	730	750	57.53	−91.65	25	$0.498_{\pm0.050\pm0.003}$
	2012.09.24	56 194.760	0.26	532	547	65.10	−125.10	9	$0.146_{\pm0.050\pm0.002}$
	2012.09.24	56 194.760	0.26	547	560	65.10	−125.10	10	$0.127_{\pm0.050\pm0.002}$
	2012.09.24	56 194.760	0.26	710	730	65.09	−125.06	39	$0.366_{\pm0.050\pm0.003}$
	2012.09.24	56 194.760	0.26	730	750	65.09	−125.06	28	$0.387_{\pm0.050\pm0.003}$
$\phi = 0.292 \pm 0.009$	2014.07.11	56 849.865	−2.14	585	600	59.09	−96.30	12	$0.312_{\pm0.025\pm0.003}$
	2014.07.11	56 849.865	−2.14	730	750	59.08	−96.26	12	$0.454_{\pm0.039\pm0.002}$
	2014.07.11	56 849.876	−1.87	585	600	60.10	−99.54	10	$0.225_{\pm0.023\pm0.002}$
	2014.07.11	56 849.876	−1.88	730	750	60.09	−99.51	12	$0.387_{\pm0.033\pm0.002}$
	2014.07.11	56 849.931	−0.57	660	680	63.80	−115.21	12	$0.262_{\pm0.022\pm0.002}$
	2014.07.11	56 849.944	−0.24	660	680	64.40	−119.09	8	$0.286_{\pm0.036\pm0.002}$
	2014.07.11	56 849.972	0.45	610	630	65.30	−127.45	7	$0.269_{\pm0.037\pm0.003}$
	2014.07.11	56 849.984	0.72	610	630	65.52	−130.73	6	$0.177_{\pm0.027\pm0.002}$
	2014.07.11	56 849.984	0.72	630	650	65.52	−130.73	6	$0.225_{\pm0.039\pm0.002}$
$\phi = 0.401 \pm 0.003$	2012.08.29	56 168.980	3.91	700	720	65.51	−172.09	22	$0.290_{\pm0.013\pm0.002}$
	2012.08.29	56 168.980	3.91	720	740	65.51	−172.09	29	$0.362_{\pm0.012\pm0.003}$
	2012.08.29	56 169.013	4.70	700	720	65.47	177.14	18	$0.309_{\pm0.017\pm0.002}$
	2012.08.29	56 169.013	4.70	720	740	65.47	177.14	24	$0.379_{\pm0.016\pm0.003}$
$\phi = 0.526 \pm 0.001$	2013.07.23	56 497.003	1.90	525	540	65.87	−145.43	3	$0.094_{\pm0.036\pm0.001}$
	2013.07.23	56 497.003	1.90	540	555	65.87	−145.43	12	$0.133_{\pm0.011\pm0.002}$
	2013.07.23	56 497.003	1.90	710	730	65.87	−145.43	11	$0.307_{\pm0.029\pm0.002}$
	2014.07.07	56 845.819	−3.51	514	527	52.67	−78.48	9	$0.307_{\pm0.036\pm0.003}$
	2014.07.07	56 845.819	−3.51	527	542	52.67	−78.48	7	$0.264_{\pm0.038\pm0.002}$
	2014.07.07	56 845.819	−3.51	695	715	52.66	−78.46	14	$0.508_{\pm0.036\pm0.003}$
	2014.07.07	56 845.831	−3.26	514	527	53.95	−81.85	8	$0.241_{\pm0.029\pm0.002}$
	2014.07.07	56 845.831	−3.26	527	542	53.95	−81.85	10	$0.268_{\pm0.026\pm0.002}$
	2014.07.07	56 845.831	−3.26	695	715	53.94	−81.84	15	$0.454_{\pm0.029\pm0.002}$
$\phi = 0.627 \pm 0.017$	2013.10.23	56 588.841	4.12	710	730	65.50	−174.91	10	$0.377_{\pm0.039\pm0.003}$
	2013.10.23	56 588.841	4.12	725	740	65.50	−174.91	10	$0.361_{\pm0.038\pm0.003}$
	2013.10.23	56 588.877	4.91	710	730	65.50	174.27	9	$0.331_{\pm0.036\pm0.003}$
	2013.10.23	56 588.877	4.91	725	740	65.50	174.27	14	$0.367_{\pm0.027\pm0.003}$
	2014.07.02	56 840.912	−1.51	580	595	61.35	−103.99	4	$0.197_{\pm0.050\pm0.002}$
	2014.07.02	56 840.912	−1.51	730	750	61.35	−103.98	7	$0.354_{\pm0.050\pm0.002}$
	2014.07.02	56 840.930	−1.13	580	595	62.46	−108.48	4	$0.207_{\pm0.050\pm0.002}$
	2014.07.02	56 840.930	−1.13	730	750	62.46	−108.47	7	$0.349_{\pm0.050\pm0.002}$

Notes. The columns give, respectively, the date, the RJD, the hour angle (HA), the minimum and maximum wavelengths over which the squared visibility is calculated, the projected baseline length Bp and its orientation PA, the signal-to-noise ratio on the fringe peak; the last column provides the calibrated squared visibility V^2 together with the statistic error on V^2, and the systematic error on V^2 (see text for details). The data are available on the Jean-Marie Mariotti Center OiDB service (http://oidb.jmmc.fr), and at the CDS.

Table A.1. continued.

	Date	RJD	HA	λ_{min}	λ_{max}	Bp	PA	S/N	$V^2_{cal\pm stat\pm syst}$
	[yyyy.mm.dd]	[days]	[hour]	[nm]	[nm]	[m]	[deg]		
$\phi = 0.741 \pm 0.003$	2012.09.27	56 197.642	−2.40	532	547	58.02	−93.06	11	0.272 $_{\pm 0.024 \pm 0.003}$
	2012.09.27	56 197.642	−2.40	547	560	58.02	−93.06	12	0.277 $_{\pm 0.022 \pm 0.003}$
	2012.09.27	56 197.642	−2.42	710	730	57.92	−92.79	33	0.459 $_{\pm 0.014 \pm 0.003}$
	2012.09.27	56 197.642	−2.42	730	750	57.92	−92.79	28	0.516 $_{\pm 0.018 \pm 0.003}$
	2012.09.27	56 197.665	−1.79	532	547	60.39	−100.54	14	0.280 $_{\pm 0.020 \pm 0.003}$
	2012.09.27	56 197.665	−1.79	547	560	60.39	−100.54	17	0.297 $_{\pm 0.018 \pm 0.003}$
	2012.09.27	56 197.665	−1.80	710	730	60.37	−100.47	30	0.459 $_{\pm 0.015 \pm 0.003}$
	2012.09.27	56 197.665	−1.80	730	750	60.37	−100.47	19	0.507 $_{\pm 0.026 \pm 0.003}$
$\phi = 0.783 \pm 0.002$	2013.10.24	56 589.603	−1.61	547	562	61.03	−102.77	12	0.275 $_{\pm 0.022 \pm 0.003}$
	2013.10.24	56 589.603	−1.61	705	725	61.03	−102.77	18	0.424 $_{\pm 0.023 \pm 0.003}$
	2013.10.24	56 589.603	−1.61	710	730	61.03	−102.77	26	0.430 $_{\pm 0.016 \pm 0.003}$
	2013.10.24	56 589.603	−1.61	725	740	61.03	−102.77	18	0.509 $_{\pm 0.028 \pm 0.003}$
	2013.10.24	56 589.603	−1.61	725	745	61.03	−102.77	22	0.461 $_{\pm 0.021 \pm 0.003}$
	2013.10.24	56 589.615	−1.35	532	547	61.83	−105.83	5	0.228 $_{\pm 0.050 \pm 0.003}$
	2013.10.24	56 589.615	−1.35	705	725	61.83	−105.83	15	0.468 $_{\pm 0.031 \pm 0.003}$
	2013.10.24	56 589.615	−1.35	710	730	61.83	−105.83	24	0.470 $_{\pm 0.019 \pm 0.003}$
	2013.10.24	56 589.615	−1.35	725	740	61.83	−105.83	15	0.471 $_{\pm 0.031 \pm 0.003}$
	2013.10.24	56 589.615	−1.35	725	745	61.83	−105.83	18	0.461 $_{\pm 0.026 \pm 0.003}$
	2013.10.24	56 589.625	−1.07	532	547	62.64	−109.25	7	0.211 $_{\pm 0.030 \pm 0.002}$
	2013.10.24	56 589.625	−1.07	705	725	62.64	−109.25	16	0.473 $_{\pm 0.029 \pm 0.003}$
	2013.10.24	56 589.625	−1.07	710	730	62.64	−109.25	14	0.463 $_{\pm 0.033 \pm 0.003}$
	2013.10.24	56 589.625	−1.07	725	740	62.64	−109.25	13	0.426 $_{\pm 0.034 \pm 0.003}$
	2013.10.24	56 589.625	−1.07	725	745	62.64	−109.25	17	0.456 $_{\pm 0.027 \pm 0.003}$
$\phi = 0.821 \pm 0.012$	2014.10.24	56 954.655	−0.29	570	585	64.32	−118.48	11	0.238 $_{\pm 0.021 \pm 0.003}$
	2014.10.24	56 954.655	−0.29	730	750	64.32	−118.47	13	0.336 $_{\pm 0.025 \pm 0.002}$
	2014.10.24	56 954.678	0.24	520	535	65.07	−124.85	7	0.145 $_{\pm 0.022 \pm 0.002}$
	2014.10.24	56 954.678	0.24	695	710	65.07	−124.84	11	0.374 $_{\pm 0.033 \pm 0.003}$
	2014.10.24	56 954.699	0.75	660	680	65.54	−131.04	17	0.297 $_{\pm 0.018 \pm 0.002}$
	2014.10.24	56 954.724	1.35	610	630	65.82	−138.49	8	0.221 $_{\pm 0.027 \pm 0.002}$
$\phi = 0.848 \pm 0.007$	2013.12.17	56 643.578	1.34	532	547	65.81	−138.43	6	0.224 $_{\pm 0.040 \pm 0.003}$
	2013.12.17	56 643.578	1.34	535	555	65.81	−138.43	11	0.210 $_{\pm 0.020 \pm 0.003}$
	2013.12.17	56 643.578	1.34	705	725	65.81	−138.41	16	0.321 $_{\pm 0.020 \pm 0.002}$
	2013.12.17	56 643.578	1.34	725	745	65.81	−138.41	14	0.388 $_{\pm 0.027 \pm 0.003}$
	2013.12.17	56 643.592	1.65	532	547	65.87	−142.23	6	0.239 $_{\pm 0.041 \pm 0.003}$
	2013.12.17	56 643.592	1.65	535	555	65.87	−142.23	6	0.194 $_{\pm 0.031 \pm 0.003}$
	2013.12.17	56 643.592	1.64	705	725	65.87	−142.21	11	0.274 $_{\pm 0.026 \pm 0.002}$
	2013.12.17	56 643.592	1.64	725	745	65.87	−142.21	14	0.359 $_{\pm 0.026 \pm 0.003}$
	2013.12.17	56 643.603	1.90	705	725	65.87	−145.54	9	0.304 $_{\pm 0.034 \pm 0.002}$
	2013.12.17	56 643.614	2.16	532	547	65.86	−148.81	6	0.220 $_{\pm 0.037 \pm 0.003}$
	2013.12.17	56 643.614	2.16	535	555	65.86	−148.81	7	0.208 $_{\pm 0.030 \pm 0.003}$
	2013.12.17	56 643.614	2.16	705	725	65.86	−148.77	8	0.332 $_{\pm 0.040 \pm 0.003}$
	2013.12.17	56 643.614	2.16	725	745	65.86	−148.77	8	0.300 $_{\pm 0.036 \pm 0.002}$
	2013.12.17	56 643.624	2.42	705	725	65.82	−152.21	6	0.385 $_{\pm 0.062 \pm 0.003}$
	2013.12.17	56 643.624	2.42	725	745	65.82	−152.21	6	0.379 $_{\pm 0.060 \pm 0.003}$
	2013.12.17	56 643.644	2.91	532	547	65.72	−158.69	5	0.190 $_{\pm 0.040 \pm 0.002}$
	2013.12.17	56 643.644	2.91	705	725	65.72	−158.66	9	0.386 $_{\pm 0.042 \pm 0.003}$
	2013.12.17	56 643.676	3.67	535	555	65.56	−168.84	8	0.203 $_{\pm 0.026 \pm 0.003}$
	2013.12.17	56 643.676	3.67	705	725	65.56	−168.81	12	0.357 $_{\pm 0.030 \pm 0.003}$
	2013.12.17	56 643.676	3.67	725	745	65.56	−168.81	13	0.391 $_{\pm 0.031 \pm 0.003}$
	2013.12.17	56 643.687	3.92	532	547	65.52	−172.21	8	0.266 $_{\pm 0.034 \pm 0.003}$
	2013.12.17	56 643.687	3.92	535	555	65.52	−172.21	6	0.207 $_{\pm 0.032 \pm 0.003}$
	2013.12.17	56 643.687	3.91	705	725	65.52	−172.18	13	0.390 $_{\pm 0.029 \pm 0.003}$
	2013.12.17	56 643.687	3.91	725	745	65.52	−172.18	15	0.370 $_{\pm 0.024 \pm 0.003}$

Table A.1. continued.

	Date [yyyy.mm.dd]	RJD [days]	HA [hour]	$\lambda_{\min}$ [nm]	$\lambda_{\max}$ [nm]	Bp [m]	PA [deg]	S/N	$V^2_{\mathrm{cal\pm stat\pm syst}}$
$\phi = 0.893 \pm 0.005$	2013.07.25	56 498.942	0.64	525	540	65.46	−129.77	8	$0.174\ _{\pm0.022\pm0.003}$
	2013.07.25	56 498.942	0.64	540	555	65.46	−129.77	9	$0.191\ _{\pm0.021\pm0.003}$
	2013.07.25	56 498.942	0.64	690	710	65.46	−129.77	16	$0.287\ _{\pm0.017\pm0.002}$
	2013.07.25	56 498.942	0.64	710	730	65.46	−129.77	15	$0.302\ _{\pm0.020\pm0.002}$
	2013.07.25	56 498.942	0.64	730	750	65.46	−129.77	15	$0.361\ _{\pm0.024\pm0.002}$
	2013.07.25	56 498.961	1.04	525	540	65.71	−134.71	5	$0.194\ _{\pm0.037\pm0.003}$
	2013.07.25	56 498.961	1.04	540	555	65.71	−134.71	7	$0.247\ _{\pm0.036\pm0.003}$
	2013.07.25	56 498.961	1.04	690	710	65.71	−134.70	11	$0.310\ _{\pm0.027\pm0.002}$
	2013.07.25	56 498.961	1.04	710	730	65.71	−134.70	11	$0.307\ _{\pm0.027\pm0.002}$
	2013.07.25	56 498.961	1.04	730	750	65.71	−134.70	11	$0.273\ _{\pm0.026\pm0.002}$
	2013.07.25	56 498.978	1.41	525	540	65.83	−139.32	7	$0.221\ _{\pm0.031\pm0.003}$
	2013.07.25	56 498.978	1.41	540	555	65.83	−139.32	11	$0.236\ _{\pm0.022\pm0.003}$
	2013.07.25	56 498.978	1.41	690	710	65.83	−139.31	17	$0.299\ _{\pm0.017\pm0.002}$
	2013.07.25	56 498.978	1.41	710	730	65.83	−139.31	13	$0.340\ _{\pm0.025\pm0.002}$
	2013.07.25	56 498.978	1.41	730	750	65.83	−139.31	20	$0.297\ _{\pm0.015\pm0.002}$
	2013.07.25	56 498.988	1.67	525	540	65.87	−142.58	9	$0.176\ _{\pm0.020\pm0.002}$
	2013.07.25	56 498.988	1.67	540	555	65.87	−142.58	12	$0.208\ _{\pm0.017\pm0.003}$
	2013.07.25	56 498.988	1.67	690	710	65.87	−142.57	22	$0.299\ _{\pm0.014\pm0.002}$
	2013.07.25	56 498.988	1.67	710	730	65.87	−142.57	15	$0.337\ _{\pm0.023\pm0.002}$
	2013.07.25	56 498.988	1.67	730	750	65.87	−142.57	19	$0.325\ _{\pm0.017\pm0.002}$
	2013.07.25	56 498.999	1.95	525	540	65.87	−146.15	11	$0.211\ _{\pm0.020\pm0.003}$
	2013.07.25	56 498.999	1.95	540	555	65.87	−146.15	12	$0.238\ _{\pm0.019\pm0.003}$
	2013.07.25	56 498.999	1.95	690	710	65.87	−146.14	21	$0.330\ _{\pm0.015\pm0.003}$
	2013.07.25	56 498.999	1.95	710	730	65.87	−146.14	25	$0.369\ _{\pm0.015\pm0.003}$
	2013.07.25	56 498.999	1.95	730	750	65.87	−146.14	18	$0.337\ _{\pm0.018\pm0.002}$
	2013.07.25	56 499.010	2.16	525	540	65.86	−148.78	9	$0.186\ _{\pm0.020\pm0.003}$
	2013.07.25	56 499.010	2.16	540	555	65.86	−148.78	10	$0.197\ _{\pm0.020\pm0.003}$
	2013.07.25	56 499.010	2.16	690	710	65.86	−148.77	12	$0.288\ _{\pm0.025\pm0.002}$
	2013.07.25	56 499.010	2.16	710	730	65.86	−148.77	13	$0.330\ _{\pm0.025\pm0.002}$
	2013.07.25	56 499.010	2.16	730	750	65.86	−148.77	14	$0.314\ _{\pm0.022\pm0.002}$
$\phi = 0.927 \pm 0.003$	2014.07.09	56 847.948	−0.29	580	595	64.33	−118.57	5	$0.239\ _{\pm0.050\pm0.002}$
	2014.07.09	56 847.948	−0.29	735	755	64.33	−118.56	7	$0.368\ _{\pm0.050\pm0.002}$
	2014.07.09	56 847.961	0.03	580	595	64.81	−122.35	4	$0.212\ _{\pm0.050\pm0.002}$
	2014.07.09	56 847.961	0.03	735	755	64.81	−122.33	8	$0.390\ _{\pm0.050\pm0.002}$
	2014.07.09	56 847.978	0.47	490	510	65.32	−127.66	3	$0.173\ _{\pm0.050\pm0.003}$
	2014.07.09	56 847.978	0.47	660	680	65.32	−127.65	7	$0.341\ _{\pm0.050\pm0.003}$
	2014.07.09	56 847.990	0.74	490	510	65.54	−130.97	4	$0.181\ _{\pm0.050\pm0.003}$
	2014.07.09	56 847.990	0.74	660	680	65.53	−130.96	6	$0.307\ _{\pm0.050\pm0.003}$
$\phi = 0.942 \pm 0.007$	2013.11.26	56 622.628	1.23	547	562	65.78	−137.04	4	$0.181\ _{\pm0.050\pm0.002}$
	2013.11.26	56 622.628	1.23	705	725	65.78	−137.03	7	$0.327\ _{\pm0.050\pm0.002}$
	2013.11.26	56 622.628	1.23	725	740	65.78	−137.03	6	$0.316\ _{\pm0.050\pm0.002}$
	2013.11.26	56 622.644	1.58	547	562	65.86	−141.35	5	$0.260\ _{\pm0.050\pm0.003}$
	2013.11.26	56 622.644	1.57	705	725	65.86	−141.26	6	$0.313\ _{\pm0.050\pm0.002}$
	2013.11.26	56 622.644	1.57	725	740	65.86	−141.26	7	$0.363\ _{\pm0.050\pm0.003}$
	2013.11.26	56 622.658	1.90	535	555	65.87	−145.46	2	$0.118\ _{\pm0.050\pm0.002}$
	2013.11.26	56 622.658	1.90	547	562	65.87	−145.46	3	$0.165\ _{\pm0.050\pm0.002}$
	2013.11.26	56 622.658	1.90	705	725	65.87	−145.45	6	$0.284\ _{\pm0.050\pm0.003}$
	2013.11.26	56 622.658	1.90	725	740	65.87	−145.45	6	$0.297\ _{\pm0.050\pm0.002}$
	2013.11.26	56 622.698	2.85	597	617	65.73	−157.82	4	$0.214\ _{\pm0.050\pm0.002}$
	2013.11.26	56 622.698	2.85	617	637	65.73	−157.82	5	$0.248\ _{\pm0.050\pm0.002}$
	2013.11.26	56 622.712	3.17	617	637	65.66	−162.08	6	$0.313\ _{\pm0.050\pm0.003}$
$\phi = 0.999 \pm 0.025$	2013.10.25	56 590.620	−1.09	705	725	62.59	−109.03	16	$0.430\ _{\pm0.027\pm0.003}$
	2013.10.25	56 590.620	−1.09	725	745	62.59	−109.03	17	$0.469\ _{\pm0.027\pm0.003}$
	2013.10.25	56 590.841	4.20	532	547	65.49	−176.10	10	$0.189\ _{\pm0.019\pm0.002}$
	2013.10.25	56 590.841	4.20	705	725	65.49	−176.09	19	$0.372\ _{\pm0.019\pm0.003}$
	2013.10.25	56 590.841	4.20	725	745	65.49	−176.09	20	$0.426\ _{\pm0.022\pm0.003}$
	2013.10.25	56 590.860	4.68	532	547	65.49	177.37	3	$0.195\ _{\pm0.024\pm0.003}$
	2013.10.25	56 590.860	4.68	705	725	65.49	177.37	14	$0.346\ _{\pm0.024\pm0.003}$
	2013.10.25	56 590.860	4.68	725	745	65.49	177.37	18	$0.382\ _{\pm0.025\pm0.003}$

Table A.2. Observing log with the S1S2 baseline.

|	Date [yyyy.mm.dd]	RJD [days]	HA [h]	λ_{min} [nm]	λ_{max} [nm]	Bp [m]	Arg [deg]	S/N	$V^2_{cal\pm stat\pm syst}$
$\phi = 0.300$	2008.08.03	54 681.988	2.36	628	632	29.01	148.13	13	0.649 $_{\pm0.037\pm0.003}$
	2008.08.03	54 681.988	2.36	654	658	29.01	148.13	15	0.763 $_{\pm0.049\pm0.003}$
$\phi = 0.543 \pm 0.009$	2008.07.30	54 677.894	−0.19	629	632	30.97	171.02	8	0.667 $_{\pm0.079\pm0.003}$
	2008.07.30	54 677.894	−0.19	654	658	30.97	171.01	11	0.694 $_{\pm0.063\pm0.003}$
	2008.07.30	54 677.958	1.37	530	533	30.08	156.84	12	0.615 $_{\pm0.049\pm0.004}$
	2008.07.30	54 677.958	1.37	553	558	30.08	156.84	13	0.629 $_{\pm0.048\pm0.004}$
$\phi = 0.666 \pm 0.006$	2008.08.05	54 683.928	1.10	554	559	30.29	159.25	12	0.619 $_{\pm0.030\pm0.004}$
	2008.08.05	54 683.974	2.18	507	510	29.24	149.68	6	0.544 $_{\pm0.096\pm0.004}$
$\phi = 0.821 \pm 0.012$	2014.10.24	56 954.792	2.99	570	585	28.10	142.69	20	0.655 $_{\pm0.033\pm0.001}$
	2014.10.24	56 954.792	2.99	730	750	28.10	142.70	23	0.752 $_{\pm0.033\pm0.001}$
	2014.10.24	56 954.812	3.49	695	710	27.25	138.53	24	0.720 $_{\pm0.030\pm0.001}$
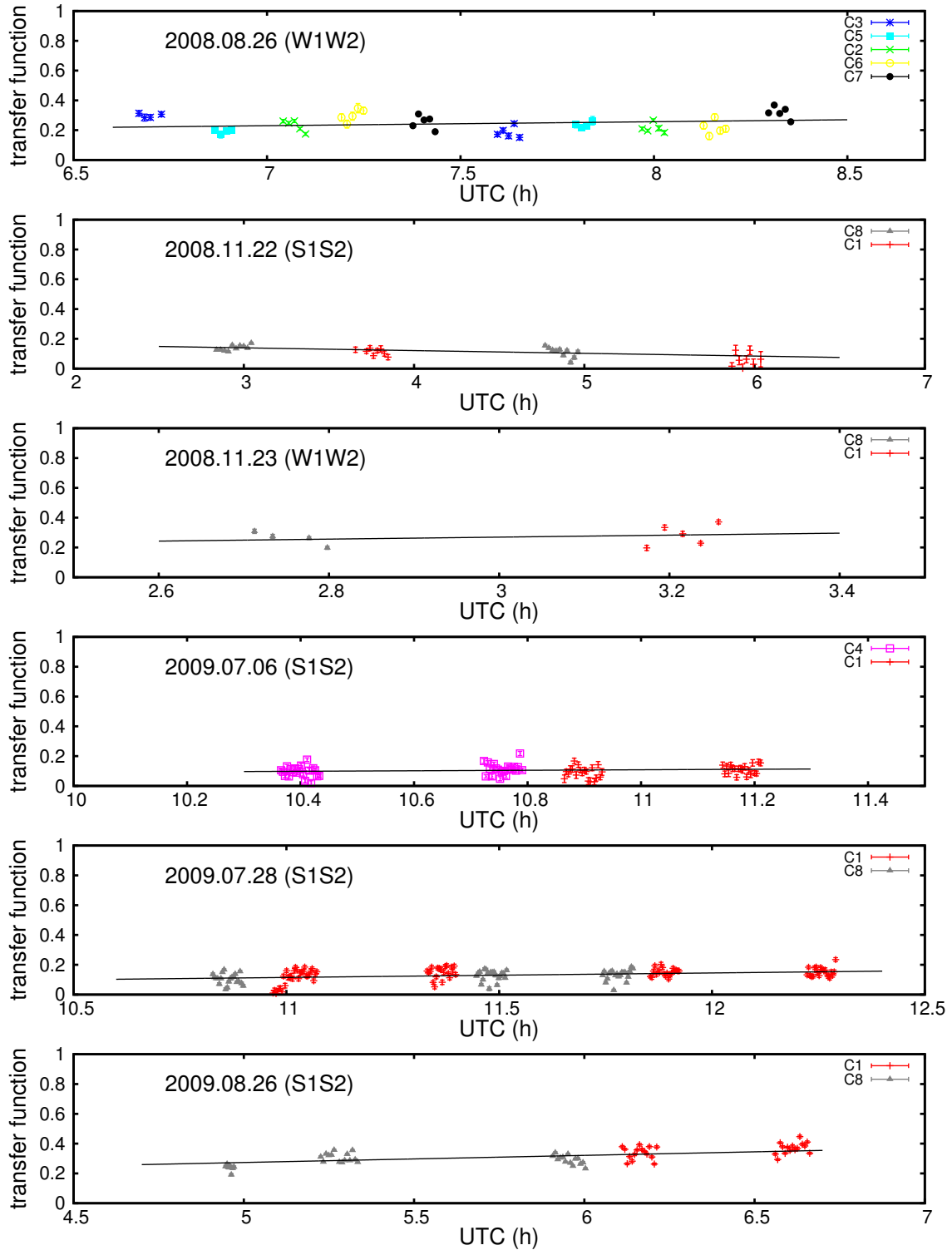
Fig. A.1. Two calibrators, C1 and C2, used to calibrate the VEGA/CHARA data of δ Cep are compared in terms of transfer functions with six other calibrators, C3 to C8 (listed in Table 2), on six different nights during 2008 and 2009. The consistency between the calibrators, which is shown by a linear fit (black line), is independent of the two-telescope baseline considered, S1S2 or W1W2.
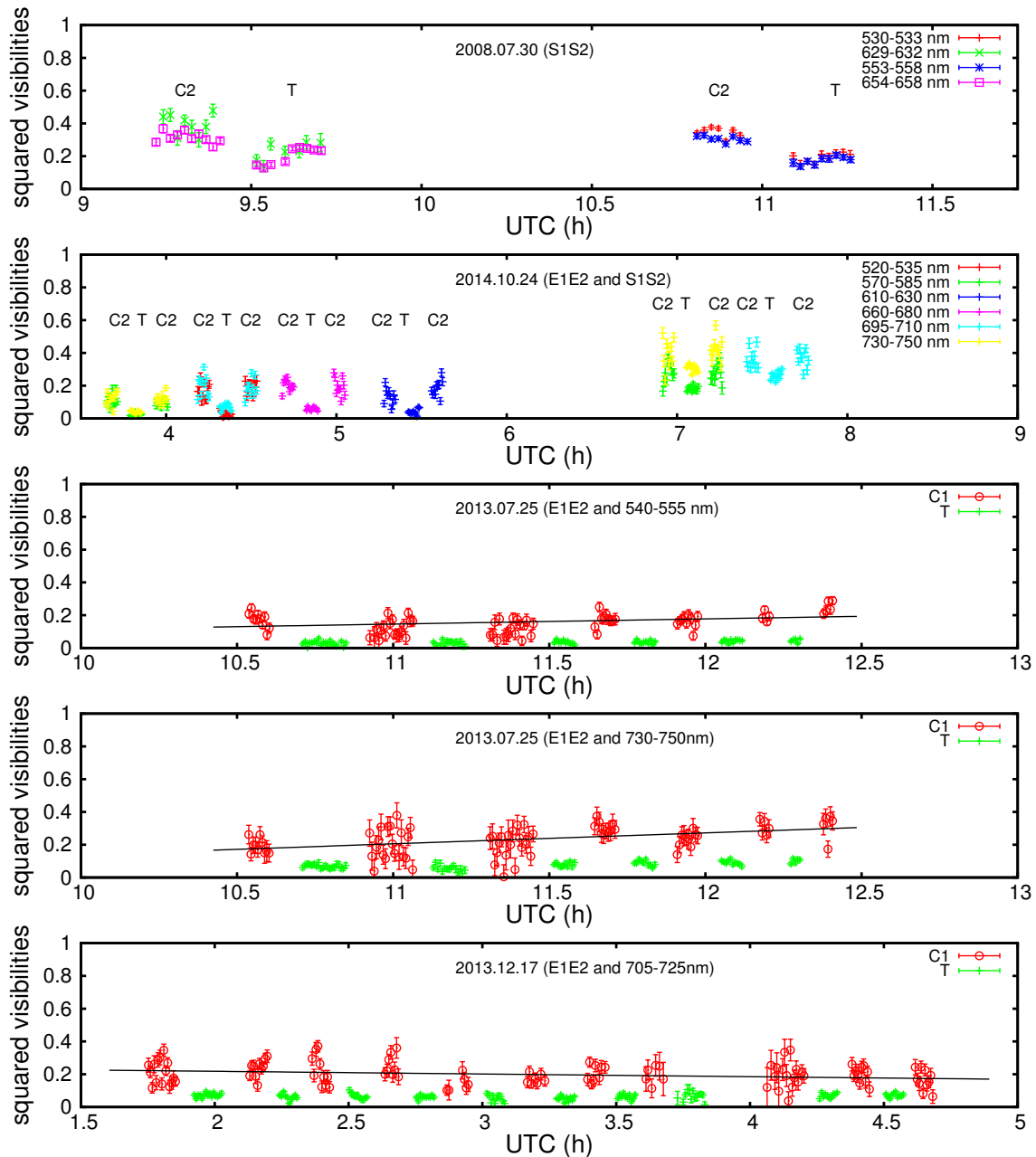
Fig. A.2. Transfer function (calculated either from the C1 or C2 calibrator) is shown together with the raw visibilities of the target (T) for four different nights in our sample, using different spectral configurations and two baselines, E1E2 and S1S2. For nights 2008 July 30 and 2014 October 24, the squared visibilities (or transfer functions) associated with calibrators C1 and C2 cannot be consistently compared as they correspond to different spectral configurations, but they are shown to illustrate the quality of the data. The 2014 October 24 observing night is the only one for which we have successive data from E1E2 (from around 3.5h to 6h in UTC) and S1S2 (from around 6.5h to 8h in UTC). For nights 2013 July 25 and 2013 December 17, the instrument configuration is the same over the entire observing time, and the stability of the transfer function is evident (black line).
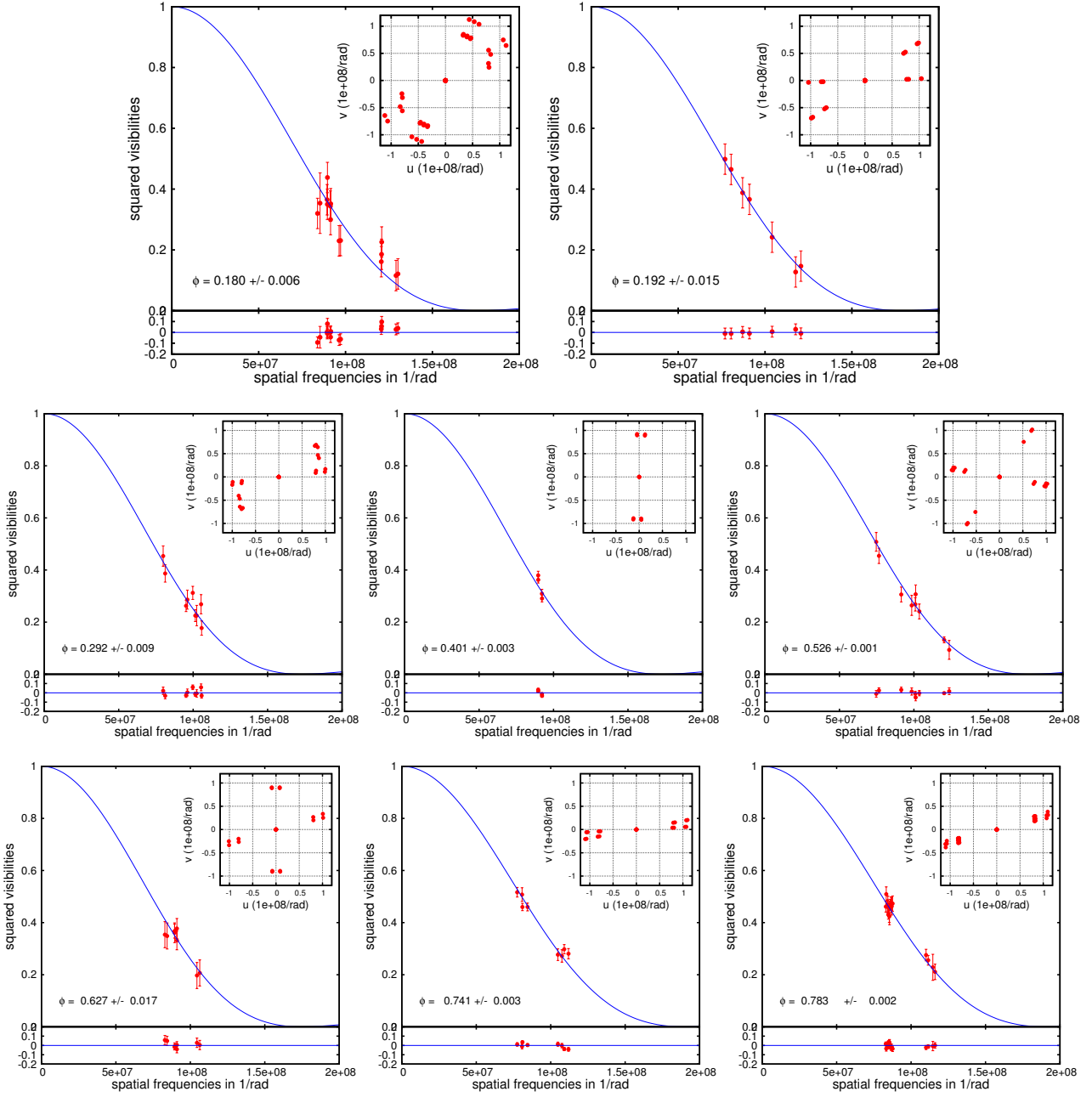
Fig. A.3. Observed calibrated squared visibilities (red dots) are plotted as a function of the spatial frequency for each pulsation phase (indicated in the lower left corner of each panel) together with the best fit of uniform disk model (solid blue line). In the upper right corner (*inset panel*) we show the corresponding (u, v) coverage.
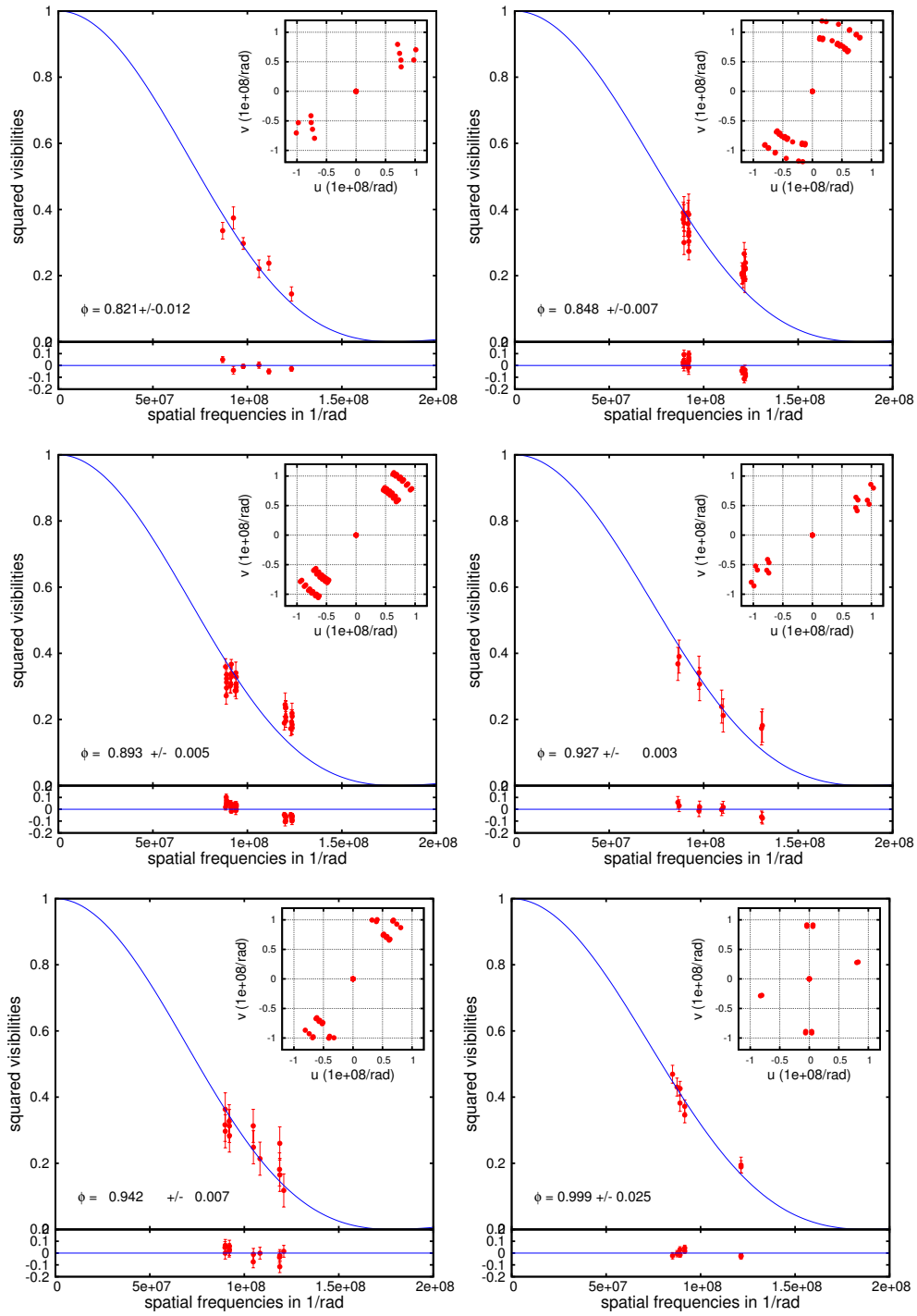
Fig. A.3. continued.